HADRON FINAL STATES IN THE TASSO DETECTOR AT PETRA*)

Dieter Notz
Deutsches Elektronen-Synchrotron DESY, Hamburg

Abstract: The DESY e^+e^- storage ring PETRA is described briefly. First results on $e^+e^- \to$ hadrons at C.M. energies of 13 GeV and 17 GeV using the TASSO detector are presented. We find R(13 GeV) = 5.6 ± 0.7 and R(17 GeV) = 4.0 ± 0.7. Comparing inclusive charged hadron spectra we observe scaling between 5 GeV and 17 GeV for $x_p > 0.2$, ($x_p = p/p_{beam}$). However the 13 GeV is above the 17 GeV cross section for smaller x_p which might be due to copious $b\bar{b}$ production. The events become more jet like with higher energies.

Résumé: Le nouvel anneau de stockage d'électrons-positrons de DESY, PETRA est décrit. Les premiers résultats de $e^+e^- \to$ hadrons aux énergies de 13 GeV et 17 GeV dans le centre de mass obtenus avec le détecteur TASSO sont présentés. Nous mesurons R(13 GeV) = 5.6 ± 0.7 et R(17 GeV) = 4.0 ± 0.7. En comparent les spectres inclusifs de hadrons chargés à 13 GeV et 17 GeV nous observons le "scaling" (l'invariance d'échelle) pour $x_p > 0.2$, ($x_p = p/p_{beam}$). Cependent la section efficace pour $x_p < 0.2$ est plus grande à 13 GeV qu'à 17 GeV ce qui pourrait être du à une abondante production de $b\bar{b}$. La structure en jet des événements devient plus nette à 17 GeV qu'à 13 GeV.

---

*) The members of the TASSO collaboration are:

R. Brandelik, W. Braunschweig, K. Gather, B. Jaax, V. Kadansky, K. Lübelsmeyer, H.-U. Martyn, G. Peise, J. Rimkus, H.G. Sander, D. Schmitz, A. Schultz von Dratzig, D. Trines, W. Wallraff, H. Boerner, H.M. Fischer, H. Hartmann, E. Hilger, W. Hillen, G. Knop, W. Korbach, B. Löhr, F. Roth, W. Rühmer, R. Wedemeyer, N. Wermes, M. Wollstadt, R. Bühring, D. Heyland, H. Hultschig, P. Joos, W. Koch, U. Kötz, H. Kowalski, A. Ladage, D. Lüke, H.L. Lynch, G. Mikenberg, D. Notz, J. Pyrlik, R. Riethmüller, M. Schliwa, P. Söding, B.H. Wiik, G. Wolf, R. Fohrmann, G. Poelz, J. Ringel, O. Römer, R. Rüsch, P. Schmüser, D.M. Binnie, P.J. Dornan, N.A. Downie, D.A. Garbutt, W.G. Jones, S.L. Lloyd, D. Pandoulas, C. Youngman, R. Barlow, R.J. Cashmore, J. Illingworth, M. Ogg, G.L. Salmon, K.W. Bell, W. Chinowsky, B. Foster, J.C. Hart, C. Proudfoot, D.R. Quarrie, D.H. Saxon, P.L. Woodworth, Y. Eisenberg, U. Karshon, E. Kogan, D. Revel, E. Ronat, A. Shapira, J. Freeman, P. Lecomte, T. Meyer, Sau Lan Wu, G. Zobernig.

1. PETRA

Fig. 1 shows the DESY accelerator complex, the synchrotron and the storage rings DORIS and PETRA. The general parameters of PETRA are summarized in Table 1 showing the design parameters and the actual values as of January 1979.

Table 1. General Parameters of PETRA

	design parameters	actual values (1/79)
Energy	5-19 GeV	8.5 GeV
Maximum luminosity per interaction point	$1.05\times10^{32}cm^{-2}sec^{-1}$ (at 15 GeV)	$5\times10^{29}cm^{-2}sec^{-1}$
Beam current (max.)	80 mA	4×2 mA
RF power	4.8 MW	
Number of bunches	1 to 4	2
Number of interaction points	6 (8)	4
Circumference	2304.0 m	
Bending radius	192.05 m	
Focusing structure	FODO	
Operating point Q_x/Q_y at 23 GeV	27.14/23.11	
Natural chromaticity ξ_x/ξ_y	-39.5/-65.3	
Amplitude function β_x^*/β_y^* at interaction point (10 m exp.space)	3.00/0.15 m	
Maximum amplitude function $\beta_{x\ max}/\beta_{y\ max}$	120/228 m	
Linear beam-beam Q shift per interaction point $\Delta Q_x/\Delta Q_y$	0.06/0.06	0.02/0.02
RF frequency	500 MHz	
Length of accelerating structures	96 m	
Injection energy	7 GeV	6.5 GeV

All three accelerators are needed when PETRA is in operation because the injection scheme is different for electrons and positrons. Electrons are accelerated by the synchrotron up to 6.5 GeV. As the positron intensity produced by LINAC II is small and the injection cycle of PETRA is of the order of 100 msec positrons are first accumulated in the storage ring DORIS at

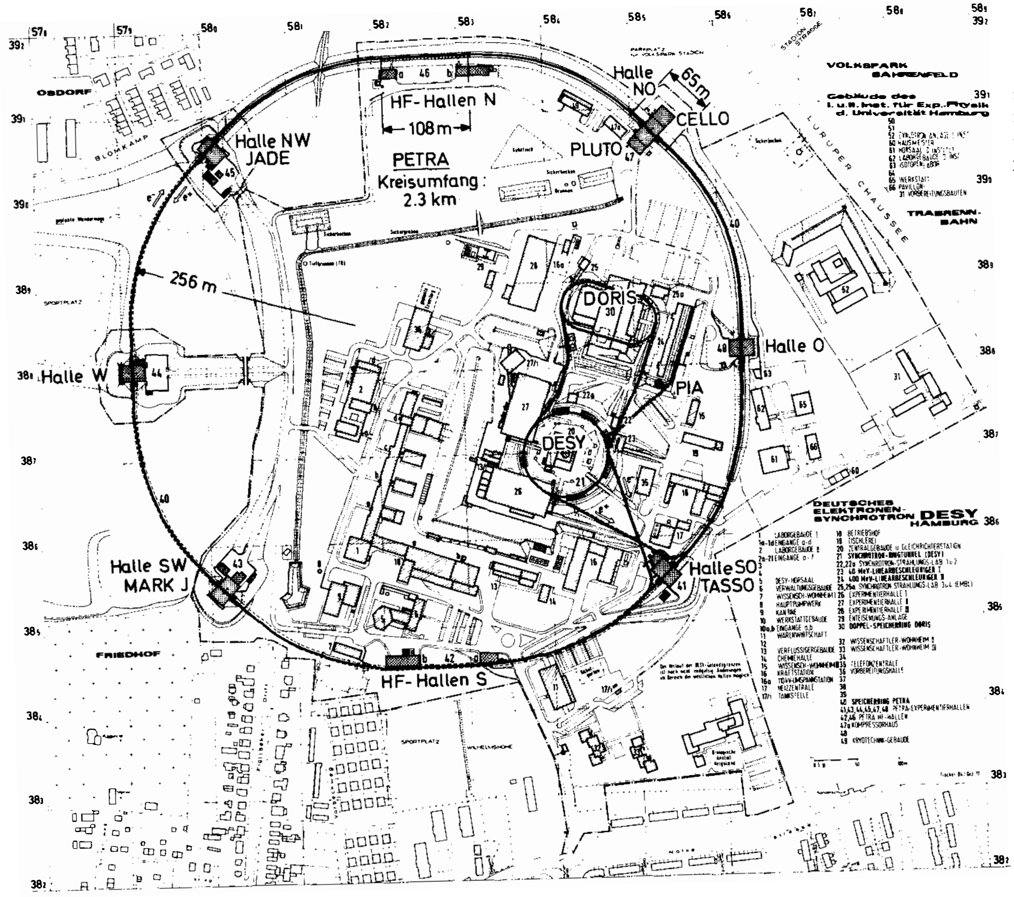

Fig.1 DESY, DORIS, PETRA and the experimental halls with the detectors PLUTO, CELLO, TASSO, MARK J and JADE. Electrons are injected by LINAC I (23) and positrons by LINAC II (24). In future positrons will be accumulated in PIA.

2.2 GeV, then transferred back to the synchrotron, accelerated to 6.5 GeV, then injected into PETRA. In order to make DORIS available for high energy physics a new small positron injection accumulator (PIA) is being built at the end of LINAC II and will come into operation within a few months.

2. Experiments at PETRA

On Fig. 1 one can see six experimental halls, four of which are equipped with 5 experiments:

Hall 5 (north-east): PLUTO (Aachen-DESY-Hamburg-Bergen-Maryland-Siegen-Wuppertal)
CELLO (DESY-Karlsruhe-Munich-Orsay-Paris-Saclay)

Hall 6 (south-east): TASSO (Aachen-Bonn-Hamburg-I.C.London-Oxford-Rutherford-Weizmann-Wisconsin)

Hall 7 (south-west): MARK J (Aachen-Amsterdam-DESY-MIT-NIKHEF-Peking)

Hall 8 (north-west): JADE (DESY-Hamburg-Heidelberg-Lancaster-Manchester-Tokyo)

Four of them use a solenoid field configuration. The respective diameters D, lengths L and Field strength B are:

	D[m]	L[m]	B[T]
CELLO	1.5	3.5	1.5
JADE	2	3.6	0.5
PLUTO	1.4	1	2
TASSO	2.7	4.5	0.5

CELLO has a 4π coverage for charged particles and neutral detection. It can separate photons from electrons with a high precision and can well distinguish between electrons, muons and hadrons.

JADE uses for track detection a drift chamber at 4 atm pressure (jet chamber) designed to measure the ionization loss for charged particles. This can be used to separate π's from K,p up to 3-5 GeV. The energy of electromagnetic showers is measured by 3048 lead glass blocks surrounding the coil and covering the endcap area. Muons are detected by drift chambers behind a rectangular muon filter.

MARK J is specialized for muon and lepton pair detection. Electromagnetic and hadron showers are detected in a combination of lead scintillator sandwich counters, drift chambers and magnetized iron sheets.

The PLUTO collaboration uses the original DORIS detector which has been upgraded for experiments at PETRA. A hadron absorber and shower counters were added for lepton and photon identification. The forward direction is covered by large angle and small angle taggers mainly to study $\gamma\gamma$ physics.

The TASSO detector uses in the central detector proportional- and drift chambers, time-of-flight and liquid argon counters for charged particle tracking, for detection of photons and for limited particle identification. In the two spectrometer arms full particle identification is provided by aerogel and Čerenkov counters, time-of-flight and shower counters and muon chambers.

PLUTO, MARK J, and TASSO were installed in September 1978 and took data during January 1979[2,3,4]. JADE was placed into the interaction region in February 1979 and CELLO will be ready in June 1979.
Two halls (east and west) are still available for experiments whereas the north and south halls house the RF.

3. The TASSO Detector

The TASSO detector is shown in fig. 2. It consists of a large magnetic solenoid, 440 cm long and with a radius of 135 cm producing a field of about 0.5 Tesla parallel to the beam axis. The coil is made of aluminium with a thickness of one radiation length. The maximum current is 5200 A. Two coils placed symmetrically with respect to the central magnet compensate the field of the solenoid. The inner part of the coil is filled with tracking chambers and scintillation counters and the outer part is surrounded by liquid argon shower counters to measure position and energy of the photons. Particles above 1 GeV are identified by two hadron arms equipped with Čerenkov-, time-of-flight- and shower counters. About 50 % of the solid angle are covered by muon chambers. A forward detector allows to measure the luminosity by small angle Bhabha scattering and to detect $\gamma\gamma$ scattering.

During the first period of data taking the detector was equipped with the inner part of the solenoid, the luminosity monitor and two muon chambers above and below the magnet.

Now we describe briefly the different components of the detector. The central part of the beam pipe is made of a 4 mm thick aluminium cylinder. The beam pipe is equipped with integrated pumps located near the exit of the solenoid and in the compensation magnets. They reach a pumping speed of 2000 torr l/sec at a pressure of 10^{-9} torr.

Four scintillation counters (5 mm thick) with a photomultiplier (56 AVP) on each end surround the beam pipe and are used in the trigger.

The proportional chamber is 140 cm long and made of styrofoam shells of 1.6 cm thickness forming 4 active gaps of 1.4 cm. The radii at the anode wires are 18.2 cm, 21.1 cm, 24.1 cm and 27.2 cm. Each gap has 480 anode wires mounted parallel to the axis and 120 inner and 120 outer cathode strips forming helices with opposite sense of rotation and a pitch of 36.5^{o}. The wires are made of 20 μ goldplated tungsten, the strips by etching copper coated Kapton film. 'Magic' gas with 75 % Argon, 25 % Isobutane, 0.25 % Freon and a small amount of Methylal is used. The chamber operates at a high voltage between 3.7 kV and 4.5 kV.

The drift chamber has a sensitive length of 323 cm with inner and outer radii of 36.6 cm and 122.2 cm. The chamber volume is divided into 6 gaps using aluminized Rohacell cylinders. These cylinders kept the chamber clean during fabrication and prevent a total break down if a wire breaks. There are 15 layers, 9 with wires parallel to the axis and 6 with sense wires orientated at an angle of approximately $\pm 4^{o}$ to the axis. The number of drift cells per layer increases from 72 for the first layer to 240 cells for the last layer. The dimension of a drift cell is the same for all layers, 1.2 cm in the radial and 3.2 cm in the azimuthal direction. The sense wires are made of 30 μ goldplated Tungsten and the potential wires of 120 μ goldplated Molybdenum which can be lengthened and pulled out if a wire breaks. A gas mixture of Argon and Methane mixed in a ratio of 9:1 is used. The operating voltage is 1.85 kV at the sense wires and -0.62 kV at the potential wires. The efficiency of the drift chamber was measured to be 99 % per layer (excluding electronic failures). The spatial resolution obtained sofar is 230 μ for high momentum tracks ($p > 2$ GeV) leading to a momentum accuracy of $\sigma/p = 2\ \% \cdot p$ for a field of 0.5 Tesla.

Inside the coil are 48 time-of-flight counters at a radius of 132 cm. The dimension of one counter is $390 \times 17 \times 2$ cm^3. Two RCA 8575 phototubes are connected to each end of a counter. The performance of the system is checked with LED's and with fiber optics connected to a spark gap.

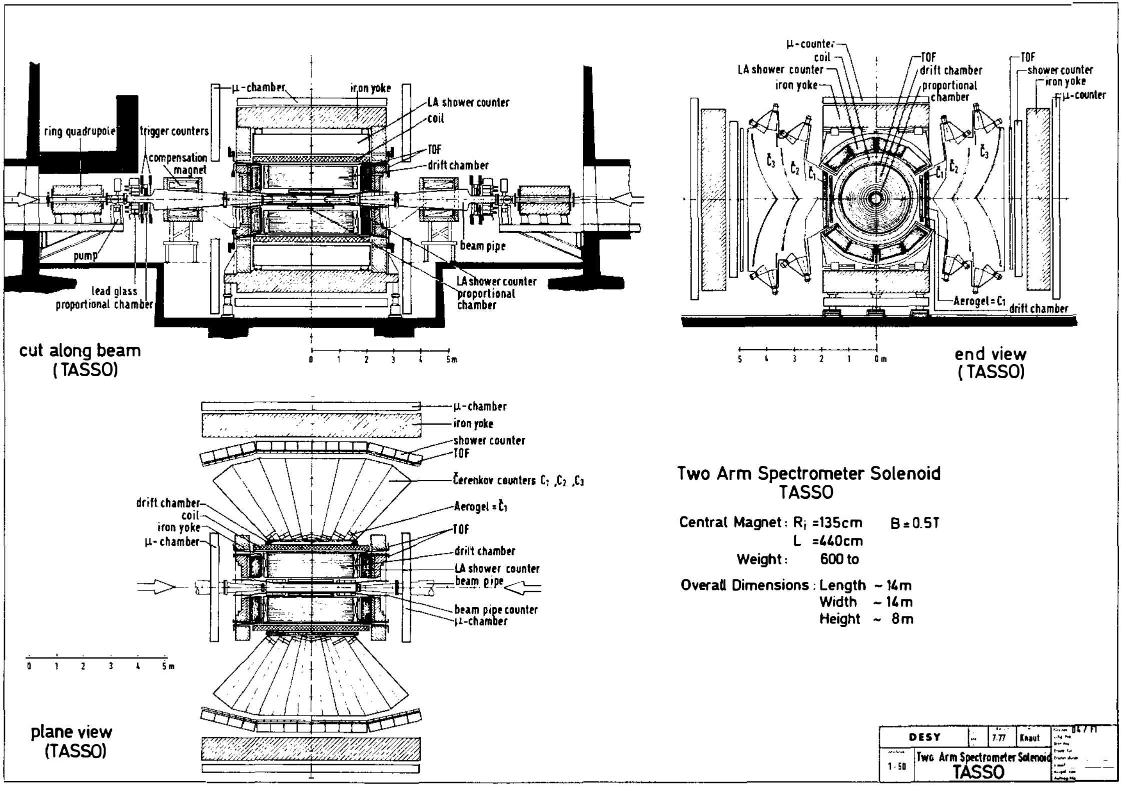

Fig. 2 The TASSO detector. Only the inner part (proportional chambers, drift chamber, TOF and muon chambers) was installed during data taking in January 1979.

The muon chambers located above and below the magnet are made of extruded Aluminium pipes with a cross section of 4 × 4 cm^2. The dimension of the chambers are 420 × 540 cm^2. The sense wires are made of 50 μ Tungsten wires and the operating voltage is typically 2.5 kV. The gas is a mixture of 80 % Argon and 20 % Methane.

The forward detector is used to measure the luminosity and to detect electrons from $\gamma\gamma$-events. Each side contains 36 lead glass blocks with 10-12 radiation lengths and 24 scintillation counters. The scattering angles seen by the forward detector range from 25 and 60 mrad.

The following components are not yet in operation and therefore described only briefly.

The liquid argon system consists of two parts: the barrel counters which surround the coil except for the area covered by the hadron arms; the end-cap counters which are located inside the coil and cover the forward and backward hemispheres. The barrel counters consist of 4 modules each roughly 440 cm long and 200 cm wide. Contrary to other liquid argon shower counters our system is segmented into towers instead of strips. The granularity of the tower arrangement is 1.5 msr in the first 5 radiation lengths and 6 msr in the remaining 9 radiation lengths. This fine granularity has two main advantages: the noise level is considerably smaller than with strips having higher capacity and photon reconstruction is much simplified. The expected energy resolution is of the order of 10 $\%/\sqrt{E/GeV}$ above 300 MeV.

To identify particles of high momentum TASSO is equipped with two arms (hadron arms) containing Cerenkov-, time-of-flight-, shower counters and muon chambers.

The Čerenkov counters are divided into 32 compartments per arm with 3 different counter types. The first counter uses as radiator aerogel with a refraction index of n = 1.02. The thresholds at 80 % efficiency are 1.0 GeV, 2.7 GeV and 6.2 GeV for π, K and p. Aerogel is a very light solid made of a macroscopic net of silicium-dioxide with air in the pores. The net structure is smaller than the wavelength of light so that the effective refraction index is an average over SiO_2 and air. The second Čerenkov counter is filled with Freon 114 (refraction index n = 1.0014, threshold 2.3 GeV, 8.3 GeV and 12.6 GeV for π, K, p) and the third one with CO_2 (refraction index n = 1.0007, threshold 4.4 GeV, 11.6 GeV for π and K).

The hadron arm time-of-flight counter system is built of 24 top and 24 bottom counters per arm. The size of each counter is 240×33 cm^2, and each counter is viewed by 2 phototubes.

The shower counters are made of 64 counters per arm with the dimensions 69×97 cm^2. They are made as a sandwich of 9 scintillator plates (1 cm thick, Plexipop) and 8 layers of lead (0.5 cm thick). The light is collected by a wavelength shifter (plexiglass dopped with BBQ) and connected to a 56 AVP multiplier. The photon energy resolution was measured to be $\Delta E/E = 18\ \% / \sqrt{E/GeV}$ for energies up to 4 GeV.

4. Installation and Data Taking

TASSO was installed during the September-October 1978 shutdown at PETRA. First tests with a single beam were carried out during November 1978 and first events were detected during a 6 days running time in December. All data reported below were taken during a two weeks period in January. At this time PETRA operated with two e^+ bunches and two e^- bunches with typical currents of 1 mA (2 mA) per bunch at 13 GeV (17 GeV) C.M. energy resulting in a typical luminosity of $2\cdot10^{29}\text{cm}^{-2}\text{sec}^{-1}$ ($5\cdot10^{29}\text{cm}^{-2}\text{sec}^{-1}$). The vacuum in our interaction region was of the order of $1\text{-}2\cdot10^{-9}$ torr.

How can one trigger the experiment? If one demands the beam crossing signal and at least one inner time-of-flight counter the rate is ~20 kHz which is much too high for transfer to the online computer. Therefore a fast hardware processor is used to search for tracks in the drift chamber (fig.3). The processor reads six of the nine zero-degree layers.

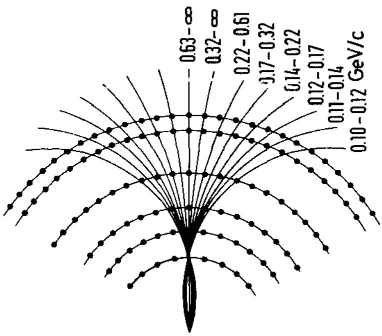

Fig.3 Masks used in the drift chamber track finding hardware processor. For all 72 reference wires of the first drift chamber layer 15 possible track configurations are tested using 6 zero-degree layers. All masks are tested in parallel so that the result is available within 4 μsec.

For each of the 72 wires of the inner layer (reference wires) 15 possible masks corresponding to different momentum bites are checked giving a total of 1080 different track masks. At this level the time information from the wires is not used. All possibilities are tested in parallel and a hardwired combination made by FPLA's (field programmable logic arrays) is called a track if at least 5 of 6 layers per mask give a hit. The minimum number of tracks above a certain momentum to be accepted is specified via a majority logic. The result of the processor is available within 4 μsec.

The following table shows how the rate is reduced if one demands a coincidence between the beam crossing signal, one time-of-flight counter and a certain number of tracks above a cut off momentum. All values are for 8.5 GeV beam energy and 10^{-9} torr vacuum.

	P_{min} > 150 MeV/c	P_{min} > 300 MeV/c
≥1 track	60 Hz	20 Hz
≥2 tracks	11 Hz	4 Hz
≥3 tracks	4 Hz	1.5 Hz

The data were collected with the following trigger: A coincidence between a beam pick up signal, any beam pipe counter, any TOF counter and more than three tracks with P_{min} > 300 MeV/c. In addition events were accepted with two tracks coplanar with the beam axis in order to detect also $e^+e^- \to e^+e^-$ and $e^+e^- \to \mu^+\mu^-$ events. A typical event is shown in fig. 4.

Roughly 650 k triggers were collected. To select multihadron events from single photon annihilation the following steps were used:

With a fast track finding program (1000 events/minute IBM 370/168 CPU time) using the minimal spanning tree method all triggers are geometrically reconstructed. 40k candidates fulfilled the selection criteria for two tracks found in the $r\phi$ plane.

In a second step 3 tracks are required in $r\phi$ and 2 tracks should have been reconstructed in all 3 coordinates $r\phi z$ and emerge from the interaction region ($d \leq 2.5$ cm, $|z| < 10$ cm). A total of 168 (143) candidates at 17 GeV (13 GeV) pass these criteria.

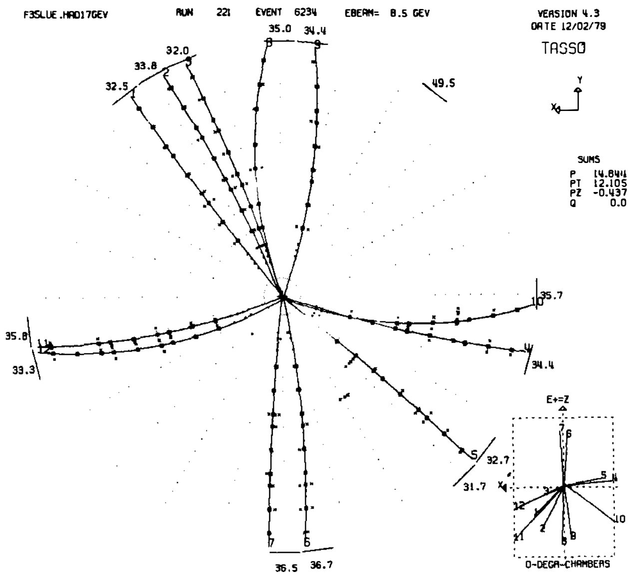

Fig. 4 A typical event at 17 GeV C.M. energy.
The first 4 layers are proportional chambers, the following 9 layers are the zero-degree drift chamber wires. The bars on the outer ring indicate the time-of-flight counters which had given a signal.

To remove beam-gas background all events are then scanned and required to satisfy the following cuts:

1) The sum of the absolute values of the momenta must be at least 3.0 GeV/c (4.0 GeV/c at 17 GeV) and the sum of momenta transverse to the beam axis above 2.5 GeV/c (3.0 GeV/c at 17 GeV).

2) At least one charged track must be in each of the 2 hemispheres oriented along the beam direction.

3) The excess of positively charged particles must be less than three.

The influence of these cuts is shown in fig. 5. Outside the interaction region (fig. 5a) triggers are caused by beam gas interaction giving low Σp_i. Comparing the charge distribution for triggers with Σp_i below 3 GeV/c (fig. 5c) and above 3 GeV/c (fig. 5d) an excess of positive charge is seen for the first class.

To be considered in the further analysis, a charged particle must have a transverse momentum above 100 MeV/c and reach at least the sixth zero-degree layer in the drift chamber. This imposes an angular cut of $|\cos\Theta| \leq 0.87$.

A total of 78 events at 13 GeV and 42 events at 17 GeV were found which satisfied the above selection criteria. To estimate the background from beam-gas interactions the whole analysis was repeated with $|z| \leq 30$ cm. This analysis resulted in 6 additional events at 13 GeV and in 3 additional events at 17 GeV due to beam gas background. After subtraction we are left with 75 events at 13 GeV and 40.5 events at 17 GeV.

These events may arise either from one-photon annihilation or from two-photon processes. The number of events expected both from the hadron-like[5)] and the pointlike[6)] contribution to the two photon effects have been estimated and found to be less than 1 event after applying the cuts described above. In the following discussion we assume that all events result from the annihilation process.

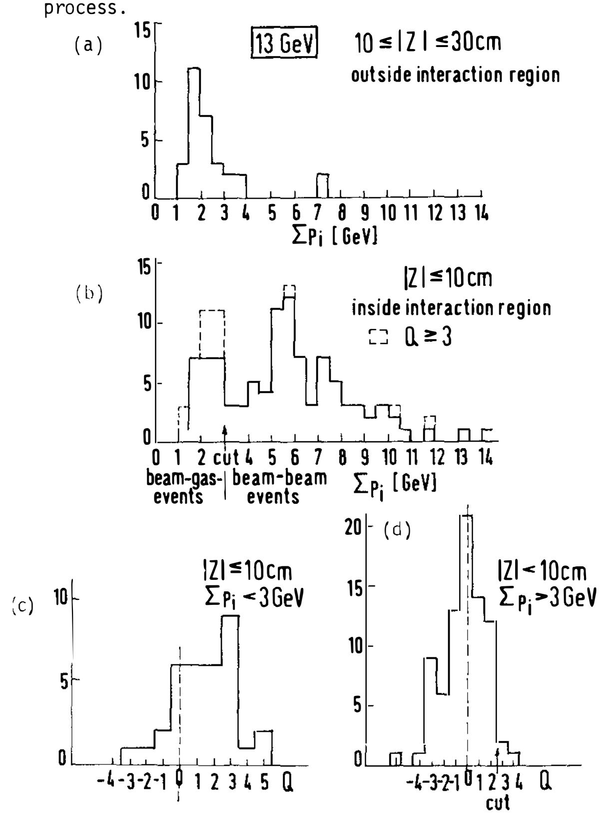

Fig. 5 Cuts to select multihadronic events from single photon annihilation.
a) Outside the interaction region beam-gas events show a low Σp_i
b) Inside the interaction region beam-gas events with charge excess $Q \geq 3$ are indicated by the dashed histogram
c) Events with $\Sigma p_i < 3$ GeV show charge excess
d) Events with $\Sigma p_i > 3$ GeV show a symmetric charge distribution.

To determine the total cross section for hadron production the contribution from τ-pair production was subtracted, and the acceptance for multihadron events evaluated.

τ-pair production will mainly populate low multiplicities[7)]; approximately one half of the τ cross section is removed by demanding a charged multiplicity of 3 or more in the trigger. The bulk of the remaining contribution is rejected by removing 4 prong events with total charge 0 having one track in one hemisphere and the other tracks in the opposite hemisphere. A total of two events at 13 GeV and one event at 17 GeV are rejected, compared to estimates of 3 and 2.5 events respectively. Higher multiplicities (>4) resulting from τ decay will contribute less than 1 event at each energy and are neglected.

5. Luminosity Measurement and Bhabha Scattering

The luminosity is determined from two independent measurements of the Bhabha cross section at small and large scattering angles. The small angle luminosity monitor consists of 4 arms with small ($4 * 16$ cm^2) and big ($9 * 19$ cm^2) scintillation counters and lead glass counters (12 radiation lengths) giving 8 possible coincidences between one small and one big counter on the opposite arm. The data are corrected for radiation effects. Large angle Bhabha events are detected in the central detector by requiring two coplanar tracks in the trigger logic. In order to compute the cross section the following corrections are applied:

1) External radiation and energy losses reduces the number of events.
2) δ-rays, trident production ($e \to e\gamma \to eee$) and internal radiation with pair production produce events with more than two tracks and are rejected by hard- and software cuts.
3) Edge effects on the collinearity cut and the limited acceptance are taken into account.

The correction factors are shown in fig.6 and the cross section is given in fig.7 together with the QED prediction.

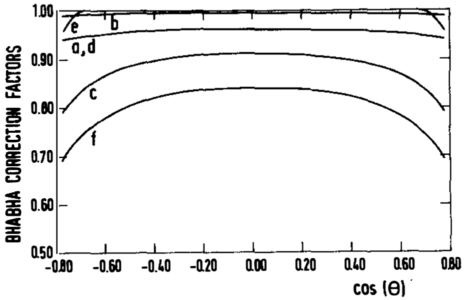

Fig.6 Correction factors for Bhabha cross section
a) external radiation energy loss
b) δ-rays
c) external cascade
d) internal γ, external pair production
e) edge effects
f) product of the correction factors a) - d)

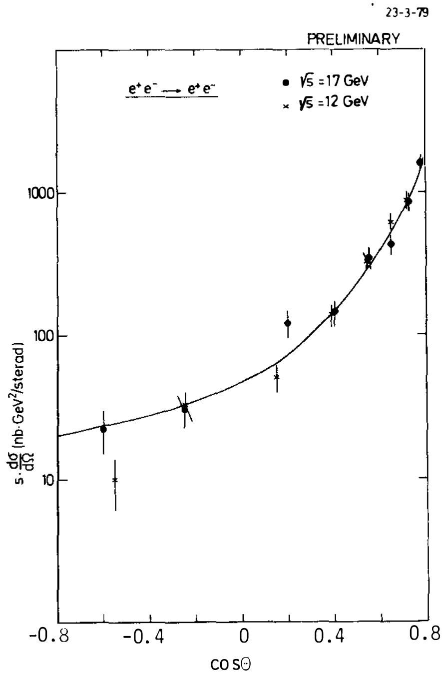

Fig. 7 Bhabha cross section s dσ/dΩ versus cosΘ and QED prediction

From the luminosity monitor we obtain an integrated luminosity of 31.0 nb^{-1} at 13 GeV and 39.2 nb^{-1} at 17 GeV. The resulting luminosity for large angle scattering (37^{0} - 143^{0}) is (29.6 ± 3.0) nb^{-1} and (39.2 ± 3.5) nb^{-1} at 13 GeV and 17 GeV respectively (statistical error only). The two measurements are in good agreement and we use the average value of 30.3 nb^{-1} at 13 GeV and 39.2 nb^{-1} at 17 GeV with an estimated systematic uncertainty of no more than 10 %.

6. Results

6.1 Total Cross Section

The total cross section devided by the muon cross section $R = \sigma_{Had}/\sigma_{\mu\mu}$ ($\sigma_{\mu\mu} = \frac{4\pi\alpha^2}{3s}$) is determined from the data in the following way:

$$\sigma_{Had} = \frac{\text{No. of events}}{\text{integrated luminosity}} \cdot \frac{f}{\varepsilon \cdot A}$$

A = Acceptance

ε = Efficiency

f = factor for radiative correction

The acceptance is determined by a Monte Carlo computation using a jet model[8,9] for the production process and propagating the events through the detector including the trigger and the cuts discussed above. The principal features of the data are consistent with the predictions from the jet model as discussed below. The computation yielded an acceptance of A = 0.77 at 13 GeV and 0.78 at 17 GeV.

The efficiency is determined by the different components having the following values:

Proportional chamber	97 %	per layer
Drift chamber including electronic failures	96 %	

Radiative corrections require reducing the observed cross sections by 8 % for both 13 and 17 GeV.

The final values of R are

$$R(13\text{ GeV}) = 5.6 \pm 0.7 \text{ and } R(17\text{ GeV}) = 4.0 \pm 0.7,$$

(statistical errors only). Changing the cuts leads to values for R in good agreement with the values listed above and we estimate that our overall systematic uncertainty including the luminosity measurement, the two-photon process, τ-pair production, and detection efficiency is no more than 20 %. The relative systematic error for the 2 energies is less than 10 %. These values for R are in reasonable agreement with the values reported by the PLUTO[3] (5.0 ± 0.5 and 4.3 ± 0.5) and MARK J[4] (4.6 ± 0.5 and 4.9 ± 0.6) collaborations.

The naive quark model predicts R = 3.7 for energies well above b threshold. The value for R at 17 GeV is in agreement with this prediction; the R value at 13 GeV could be somewhat higher (fig. 8).

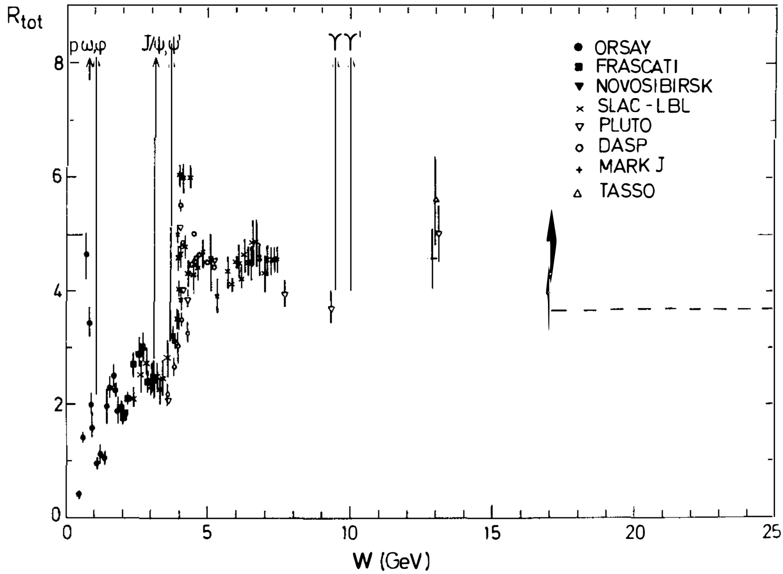

Fig. 8 Total hadronic cross section divided by pointlike muon cross section versus C.M. energy. Above b threshold the naive quark model predicts R = 3.7 as indicated by the dashed line.

6.2 Sphericity and thrust

It has been conjectured that hadron production in e^+e^- annihilation proceeds by quark pair production with the quark fragmenting into two roughly collinear jets of hadrons. Data[10)] at lower energies from SPEAR and DORIS support this picture. We have analyzed our data in order to see if these features persist also at PETRA energies.

Several variables, which can be used to characterize the production process have been proposed. Here we evaluate the data using sphericity[11)] and thrust[12)] defined as follows:

Sphericity $S = \frac{3}{2} \min \frac{\sum (p_\perp^i)^2}{\sum (p^i)^2}$. Here p^i is the momentum of a particle and $p_\perp^i$ is its transverse component with respect to a given axis. S approaches 1 for an isotropic event and 0 for a jet like event.

Thrust[13] $T = \max \frac{\sum |p_{\parallel}^i|}{\sum p^i}$, where $p_{\parallel}^i$ is the momentum component along a given axis. Both sums are taken over all observed particles. T is a measure of the maximum directed momentum. It approaches $\frac{1}{2}$ for an isotropic event and 1 for a jet like event.

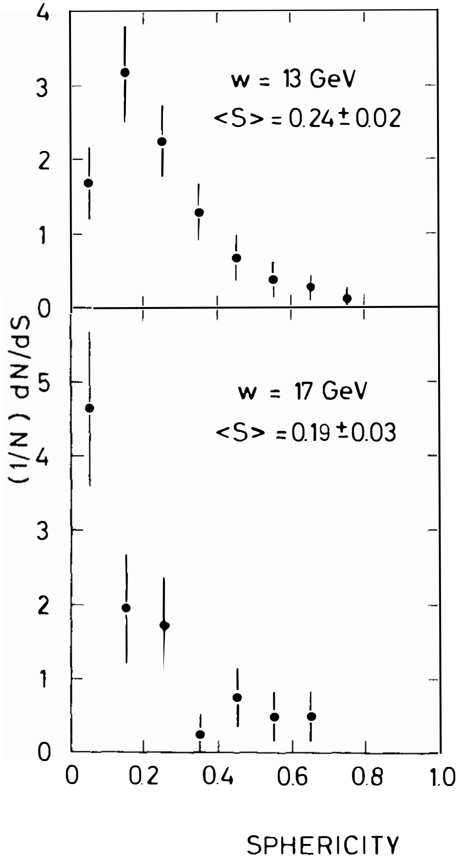

Fig.9 The sphericity distribution (1/N)dN/dS of the data at 13 GeV and 17 GeV. The distributions are normalized to the total number of events N observed at each energy.

The normalized sphericity distributions (1/N) dN/dS are plotted in fig. 9 for 13 GeV and 17 GeV separately. The distributions peak at low S and shrink with increasing C.M. energy as expected for jet like events.

At 13 GeV the mean value of the sphericity is 0.24 ± 0.02 compared to 0.19 ± 0.03 at 17 GeV. These values are in agreement with the values obtained by PLUTO[3] (0.26 ± 0.02 and 0.22 ± 0.02) at the same energies. The 17 GeV value is smaller than the value of 0.27 ± 0.01 found[13] at 9.4 GeV. The mean thrust values are 0.85 ± 0.01 and 0.87 ± 0.01 at 13 GeV and 17 GeV respectively, compared to 0.824 ± 0.005 at 9.4 GeV[13]. Fig.10 shows the energy dependence of S as measured in this and the other experiments. The average S is decreasing from a value of 0.4 at 4 GeV to 0.2 at 17 GeV. This demonstrates that the events become more jetlike as the energy increases. This figure also indicates the expected rise of sphericity if the threshold for pair producing the sixth quark t is passed. The data indicate that 17 GeV is most likely below the $t\bar{t}$ threshold.

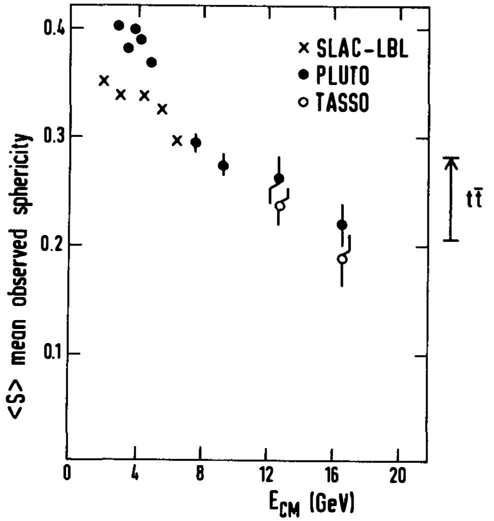

Fig.10 Energy dependence of the mean sphericity. With increasing energy the events become more jet-like. The expected rise of the mean spericity due to $t\bar{t}$ production at threshold is indicated on the right side.

6.3 Transverse Momenta and Jet Angular Distribution

The increasing jettines is a consequence of the fact that the transverse momentum with respect to the jet axis is constant or grows only slowly with energy, whereas the longitudinal momentum increases rapidly with energy. We have determined the average values $\langle p_\perp \rangle$ and $\langle p_{\parallel} \rangle$ defined with respect to the sphericity jet axis. We find without correcting for acceptance effects $\langle p_\perp \rangle = 0.31 \pm 0.01$ GeV/c at 13 GeV and 0.34 ± 0.01 GeV/c at 17 GeV. The average value of the longitudinal momentum with respect to the axis increases from 0.68 ± 0.05 GeV/c at 13 GeV to 0.92 ± 0.05 GeV/c at 17 GeV.

The simple jet picture with spin 1/2 quarks predicts that the angular distribution of the jet axis should be proportional to $1 + \cos^2\Theta$. The angular distribution of the jet axis (defined by sphericity) has been plotted in fig. 11 for the combined 13 GeV and 17 GeV data. A maximum likelihood fit to the form $1 + a\cos^2\Theta$ yields $a = 1.7 \pm 0.7$, consistent with $1 + \cos^2\Theta$.

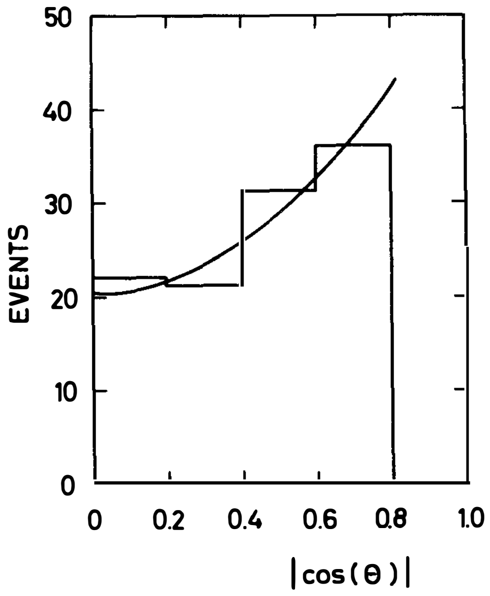

Fig. 11 The angular distribution of the sphericity axis for the 13 GeV and 17 GeV data summed. Plotted is the number of events versus cosΘ. The solid line is a best fit to the data of the form 1 + acosΘ² with a = 1.7 ± 0.7

6.4 Inclusive Hadron Production and Test for Scaling

Approximate scale invariance is an important property of deep inelastic electron hadron scattering. In analogy one expects scale invariance to hold also in e^+e^- annihilation. For high particle energies E >> m scale invariance leads to the following expression[14)] for the inclusive cross section as a function of the scaling variable $x = 2E/\sqrt{s}$:

$$\frac{d\sigma}{dx} = 3\sigma_{\mu\mu} \; x \; (- \bar{F}_1(x) + \frac{1}{6} \; x \; \bar{F}_2(x))$$

Here $\bar{F}_1$ and $\bar{F}_2$ are the two independent structure functions.

If scale invariance is fulfilled the shape of $d\sigma/dx$ should have the energy dependence as $\sigma_{\mu\mu} \sim 1/s$ and therefore $s \cdot d\sigma/dx$ should be energy independent. Since the particle mass is not determined, we use the quantity $s \; d\sigma/dx_p$ with $x_p = p/p_{beam}$. The inclusive cross sections are determined by using the detection efficiency computed with the jet model[8,9)]. The data are corrected for losses due to decay in flight and absorption, assuming the particles to be pions. The decay corrections are less than 9 % and the absorption leads to a correction on the average of 4 %. A correction is applied for the beam gas contribution. The inclusive cross sections measured at 13 and 17 GeV are plotted in fig. 12. Also shown are the data measured by the DASP collaboration[15] at 5 GeV.

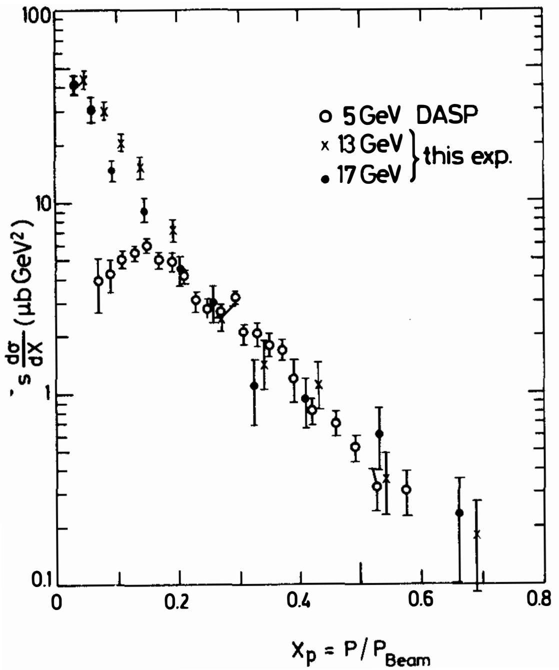

Fig.12 The inclusive cross section $s\, d\sigma/dx_p$ summed over all charged hadrons versus $x_p=p/p_{beam}$ at 13 GeV and 17 GeV. The data are compared with the cross section measured by the DASP collaboration[15]. Below $x_p < 0.2$ the 13 GeV data are above the 17 GeV data.

The data are consistent with scaling for $x_p \geq 0.2$ and C.M. energies between 5.0 GeV and 17 GeV. The cross sections at 13 GeV and 17 GeV are well above the data at 5 GeV for $x_p < 0.2$. Such a violation of scaling is expected and it gives rise to increase in multiplicity with s. However, at small x_p ($x_p \leq 0.2$) the cross section at 13 GeV is about 40 % above the cross section at 17 GeV, which is a 2 standard deviation effect, including a systematic uncertainty of 10 % in the relative normalization. This excess at small x_p is surprising since from the energy dependence one expects an effect in the opposite direction. This and the large R value observed at 13 GeV is reminiscent of the behaviour seen above charm threshold in the 4 GeV region, and it might indicate copious $b\bar{b}$ production.

If we plot the same data in terms of the invariant cross section

$$E\,\frac{d^3\sigma}{dp^3} = \frac{E}{4\pi p^2}\,\frac{d\sigma}{dp}$$

the data below 4.5 GeV can be approximated by an exponential:

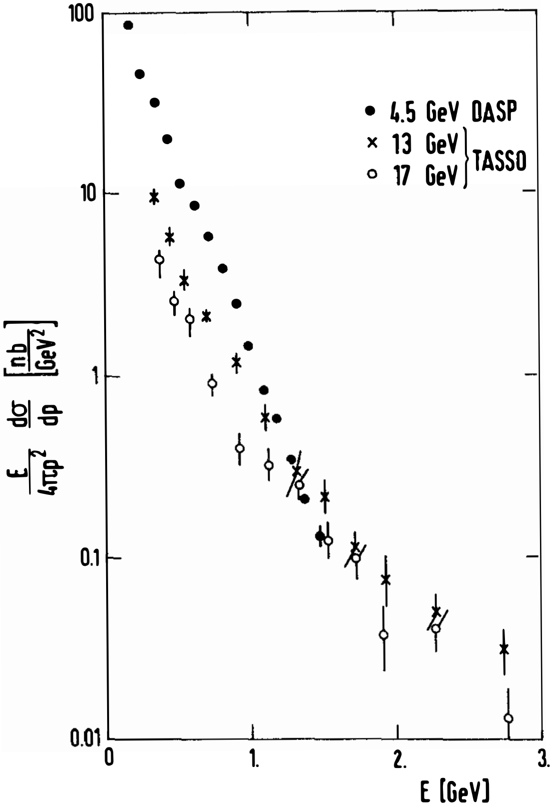

Fig.13 The invariant cross section $E/4\pi p^2\ d\sigma/dp$ summed over all charged hadrons versus E. The hadrons are assumed being pions. At high energies the data cannot be described by a single exponential function.

$$\frac{E}{4\pi p^2}\,\frac{d\sigma}{dp} \sim \exp(-bE),$$

where b is of the order 4.5 - 5.5 GeV^{-1}. If scale invariance holds b should decrease with increasing energy $b \sim \frac{1}{\sqrt{s}}$ because

$$\frac{E}{4\pi p^2}\frac{d\sigma}{dp} \sim \frac{1}{sx}\frac{d\sigma}{dx} \sim \exp(-bE)$$

$$\underbrace{s\,\frac{d\sigma}{dx}}_{\text{invariant}} \sim s^2 \times \exp(-bE) = s^2 \times \exp(\underbrace{-b\,\frac{\sqrt{s}}{2}}_{\text{invariant}}\,x)$$

Fig.13 shows the DASP data at 5 GeV[15)] and our data at 13 GeV and 17 GeV. The data at higher energies cannot be described by a single exponential. Two exponentials with slope 4 and 1.8 are needed. One possible explanation of this behaviour might be illustrated in the following figure:

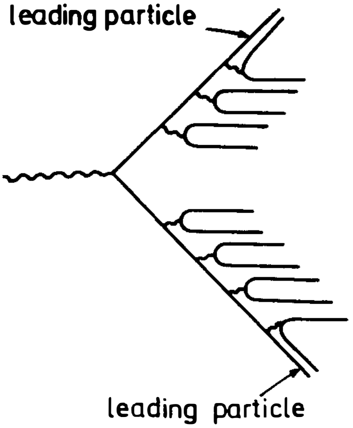

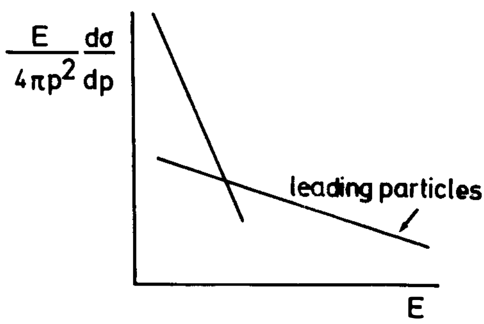

Quarks fragment into a number of physical particles. At high C.M. energies leading particles carry a larger fraction of the quark momentum than the other particles made of quarks from the sea. It appears from fig. 13 that at 17 GeV leading particles are dominant above ~1 - 1.5 GeV.

7. Conclusions

- Our measurement of R at 17 GeV C.M. energy is consistent with the naive model prediction for u, d, s, c, b quarks. The value at 13 GeV is perhaps somewhat higher.
- The measured average sphericity shows that events become more jet-like at higher energies.
- At 17 GeV the $t\bar{t}$ threshold is probably not yet reached.

- The jet angular distribution is consistent with the quark model picture where hadrons are produced by a pair of spin $\frac{1}{2}$ quarks.
- The single inclusive spectra show scaling for $x > 0.2$ between 5 and 17 GeV.
- At 13 GeV a sizable fraction of $b\bar{b}$ production may be present.

References

1) PETRA Report, updated version of the PETRA proposal, DESY, February 1976

2) TASSO Collaboration, R. Brandelik et al., DESY Report 79/11 (1979)

3) PLUTO Collaboration, Ch. Berger et al., DESY Report 79/11 (1979)

4) MARK-J Collaboration, D. Barber et al., MIT-LNS 100 (1979)

5) J. Parisi, N. Arteago-Romero, A. Jaccarini, P. Kessler, Phys. Rev. D4 (1971) 2927
S.J. Brodsky, T. Kinoshita and H. Terazawa, Phys. Rev. D4 (1971) 1532

6) S.J. Brodsky, T. de Grand, J.F. Gunion and J.H. Weis, Phys. Rev. Lett. 41 (1978) 672

7) For a review see
G.J. Feldman - Invited paper at the XIX International Conference on High Energy Physics, August 23-30, 1978, Tokyo, Japan

8) B. Anderson, G. Gustafson and C. Peterson, Nucl. Phys. B135 (1978) 273

9) R.D. Field and R.P. Feynmann, Nucl. Phys. B136 (1978) 1

10) R.F. Schwitters et al., Phys. Rev. Lett. 35 (1975) 1230
G.G. Hanson et al., Phys. Rev. Lett. 35 (1975) 1609
G.G. Hanson, Proceedings of 13th Rencontre de Moriond, edited by J. Tran Thanh Van, Vol. II p.15 and SLAC-PUB-2118 (1978)
Ch. Berger et al., Phys. Lett. B78 (1978) 176

11) J.D. Bjorken and S.J. Brodsky, Phys. Rev. D1 (1970) 1416

12) S. Brandt et al., Phys. Lett. 12 (1964) 57
E. Fahri, Phys. Rev. Lett. 39 (1977) 1587
A. de Rujula et al., Nucl. Phys. B138 (1978) 387

13) PLUTO Collaboration, Ch. Berger et al., Phys. Lett. 78B (1978) 176

14) see e.g. S. Drell, D. Levy and T.M. Yan, Phys. Rev. 187 (1969) 2159; D1 (1970) 1035, 1617, 2402

15) DASP Collaboration, R. Brandelik et al., Phys. Lett. 67B (1977) 358, DESY Report 78/50 (1978) and Nucl. Phys. B148 (1979) 189.